Accelerating seismic fault and stratigraphy interpretation w deep CNNs: A case study of the Taranaki Basin, New Zealand

Haibin Di[1], Leigh Truelove[1], Cen Li[1], and Aria Abubakar[1]

https://doi.org/10.1190/tle39100727.1

Abstract

Accurate mapping of structural faults and stratigraphic sequences is essential to the success of subsurface interpretation, geologic modeling, reservoir characterization, stress history analysis, and resource recovery estimation. In the past decades, manual interpretation assisted by computational tools — i.e., seismic attribute analysis — has been commonly used to deliver the most reliable seismic interpretation. Because of the dramatic increase in seismic data size, the efficiency of this process is challenged. The process has also become overly time-intensive and subject to bias from seismic interpreters. In this study, we implement deep convolutional neural networks (CNNs) for automating the interpretation of faults and stratigraphies on the Opunake-3D seismic data set over the Taranaki Basin of New Zealand. In general, both the fault and stratigraphy interpretation are formulated as problems of image segmentation, and each workflow integrates two deep CNNs. Their specific implementation varies in the following three aspects. First, the fault detection is binary, whereas the stratigraphy interpretation targets multiple classes depending on the sequences of interest to seismic interpreters. Second, while the fault CNN utilizes only the seismic amplitude for its learning, the stratigraphy CNN additionally utilizes the fault probability to serve as a structural constraint on the near-fault zones. Third and more innovatively, for enhancing the lateral consistency and reducing artifacts of machine prediction, the fault workflow incorporates a component of horizontal fault grouping, while the stratigraphy workflow incorporates a component of feature self-learning of a seismic data set. With seven of 765 inlines and 23 of 2233 crosslines manually annotated, which is only about 1% of the available seismic data, the fault and four sequences are well interpreted throughout the entire seismic survey. The results not only match the seismic images, but more importantly they support the graben structure as documented in the Taranaki Basin.

Introduction

The Taranaki Basin is currently the only producing basin in New Zealand. It covers approximately 330,000 km^2 and is located to the west of the North Island. It is an asymmetric basin that consists of up to 8 km of Upper Cretaceous to Quaternary sedimentary fill covering approximately 100,000 km^2 of shelf and continental slope, west of the central-western North Island (Figures 1 and 2, King and Thrasher, 1996; O'Neill et al., 2018; Mattos et al., 2019). The basin has more than 400 exploration and productions wells located both onshore and offshore; however, the limit of drilling exploration has been reached at the edge of the continental shelf. The basin has two major regions subdivided by the Cape Egmont Fault Zone: the Western Platform consisting of relatively undeformed strata and the Eastern Mobile Belt containing significantly more deformed features (King and Thrasher, 1996). The Eastern Mobile Belt is further subdivided into two dominant structural features: the Manaia Anticline and the Taranaki Fault, which bounds the Taranaki Basin to the east (Holt and Stern, 1991) and thrusts basement over Neogene and older formations. These structures may have formed during the Late Eocene (Stagpoole and Nicol, 2008) and certainly by the Early Miocene (Nelson et al., 1994; King and Thrasher, 1996; Kamp et al., 2004).

The Eastern Mobile Belt has three distinct geologic provinces: a Northern Graben, a Central Graben, and the buried Miocene Mohakatino Volcanic Centre (Figures 1 and 2, Neall et al., 1986; Stagpoole and Funnell, 2001; Hansen and Kamp, 2004). The complex deformation history of the Eastern Mobile Belt includes extensional episodes that were associated with basin subsidence and compression between the Australian and Pacific plates occurring from Late Cretaceous to Early Eocene (Holt and Stern, 1991, 1994; King and Thrasher, 1996; Nicol et al., 2005; Stagpoole and

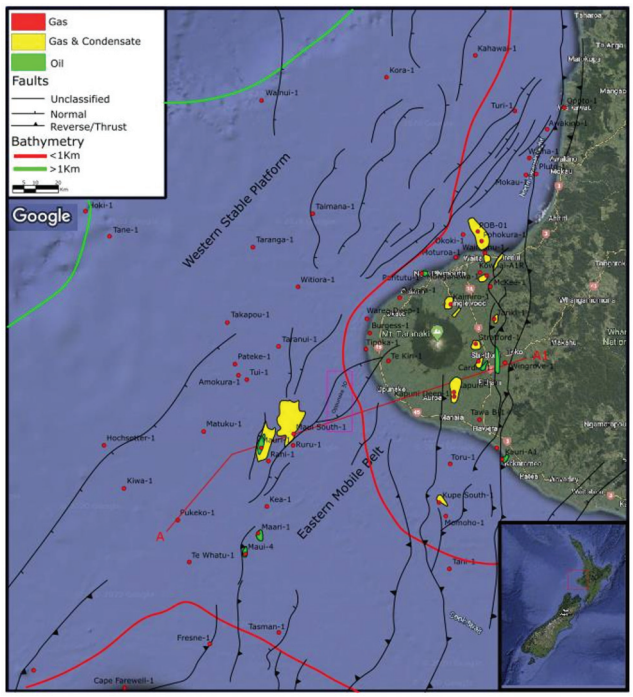

Figure 1. Map view of the Taranaki Basin displaying key wells, producing fields, structure, and bathymetry. Modified from King and Thrasher (1996) and O'Neil et al. (2018). Base map developed from Google Earth.

[1]Schlumberger, Houston, Texas, USA, and West Sussex, Gatwick, UK. E-mail: hdi@slb.com; ltruelove@slb.com; cenli@slb.com; aabubakar@slb.com.

Nicol, 2008; Giba et al., 2010). The Central Graben lies mostly south of the Taranaki Peninsula between the faulted Cape Egmont high in the west and the Manaia Anticline in the east. This deep graben contains thick, mature Jurassic source rocks that are typically marine in origin with some coal measures. These contributed to the Maui and Maari-Manaia fields. Reservoir rocks are characterized by terrestrial to near-shore sandstones, turbidites, and volcaniclastics, which are common at several levels in the Cretaceous and Cenozoic (Figure 2), with the vast majority of reservoirs producing largely oil, gas-condensate, and oil-gas.

In the past decades, enormous efforts have been devoted into computer-aided seismic interpretation, including fault detection, horizon tracking, facies analysis, etc. These tools have been or could be used for fault and stratigraphy interpretation of the Taranaki Basin. Specifically, a fault is associated with the distortions in geologic layers. In seismic, such distortion is characterized as lateral variation of seismic reflection. Correspondingly, both the discontinuity and geometric attributes highlight the faults by quantifying the distortion in certain ways. These attributes include but are not limited to coherence (Bahorich and Farmer, 1995), semblance (Marfurt et al., 1998), similarity (Tingdahl and de Rooij, 2005), variance (van Bemmel and Pepper, 2000), fault likelihood (Hale, 2013), Canny edge detection (Di and Gao, 2014), curvature (Roberts, 2001; Al-Dossary and Marfurt, 2006), and flexure (Gao and Di, 2015; Di and Gao, 2017). The stratigraphy interpretation aims at delineating multiple stratigraphic sequences that are visible in seismic and important in geology. Compared to fault detection, stratigraphy interpretation is more complicated, and the traditional approach integrates horizon tracking and geologic modeling. While the step of horizon tracking picks a set of seismic horizons to represent the important geologic boundaries, the step of geologic modeling provides a mathematical solution for stacking the picked seismic horizons in 3D space and reconstructing the sequence model by following the fundamental geologic rules (e.g., no horizon crossing). Most of the existing horizon trackers work as seeded autotracking based on the lateral continuity of seismic signals such as amplitude and gradient (e.g., Harrigan et al., 1992; Leggett et al., 1996; Huang, 1997; Höcker and Fehmers, 2002; Faraklioti and Petrou, 2004; Yu et al., 2008, 2011; Patel et al., 2010; Herron, 2011, 2015; Gramstad and Bakke, 2012; Wu and Hale, 2015). It has been well tested that the performance of such automatic horizon tracking greatly depends on the quality of seismic horizons and works effectively for reflections with strong amplitude, high signal-to-noise ratio (S/N), and high degree of lateral continuity (Herron, 2015). However, in the presence of structural complexities such as faulting, the quality of horizons is often degraded as low amplitude, low S/N, and/or low degree of lateral continuity, causing troubles in autotracking these horizons and building the corresponding stratigraphy framework.

The recent success of machine learning, particularly the convolutional neural network (CNN), in image processing (e.g., Zeiler et al., 2011; Long et al., 2015; Noh et al., 2015; Ronneberger et al., 2015; Badrinarayanan et al., 2017) has brought new insights and tools into the vision of seismic interpreters, and enormous work has been presented on efficiently utilizing the deep CNNs for resolving the typical problems in seismic pattern recognition and interpretation, such as salt-body delineation, fault detection, and facies analysis (e.g., Huang et al., 2017; Alaudah et al., 2018, 2019; AlRegib et al., 2018; Di et al., 2018, 2019, 2020; Guitton, 2018; Shi et al., 2018; Waldeland et al., 2018; Wang et al., 2018; Xiong et al., 2018; Li et al., 2019; H. Wu et al., 2019; X. Wu et al., 2019). For example, Guitton (2018) and X. Wu et al. (2019) mapped the faults in the Taranaki Basin using deep CNNs. To date, however, there have been no published studies on machine learning-assisted stratigraphy interpretation in this area.

In this study, we implement two workflows powered by the deep CNNs for seismic fault and stratigraphy interpretation, respectively, and apply them to the Opunake-3D seismic data set for interpreting the faults and four stratigraphic sequences in the Taranaki Basin, New Zealand.

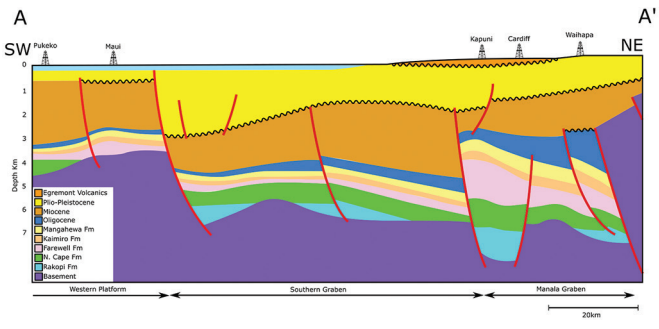

Figure 2. The schematic cross section through A-A' showing the broad stratigraphy of the Eastern Mobile Belt. Modified from King and Thrasher (1996) and O'Neil et al. (2018).

Opunake-3D seismic

The Opunake-3D seismic volume data provided by the New Zealand Crown Minerals is a prestack migrated final volume. It is located just within the Central Graben (Figure 1). The volume consists of 765 inlines and 2233 crosslines, covers an area of 215 km^2, and is acquired in 50–120 m water depth. The seismic quality is variable with the shallower sections showing well-defined reflectors with clear fault compartmentalization, while the deeper section loses most clarity with almost all the reflector definition being obscured. Simple attribute analysis using a Gaussian (structural) smoothing and variance (coherence) shows the low signal-to-noise characteristics of the deeper sequence. Therefore, this makes interpretation of the deeper (basement) sequences far harder, and so the focus for this area must be on the shallower, faulted sequences.

Training labels

The Opunake-3D seismic volume has been a target for testing fault identification workflows using machine learning in the past, and as such there are several results available for comparison (Guitton, 2018; X. Wu et al., 2019). This study extends the scope to both fault and stratigraphy interpretation, and correspondingly a set of vertical sections are interpreted manually from the volume as "supervised" labels for the machine learning algorithms.

DOI:10.1190/tle39100727.1

Given the 3D nature of seismic data, both inline and crossline directions were selected from the Opunake-3D volume at a line spacing of 100 and 200, respectively, meaning that seven inlines and 23 crosslines were picked manually as training labels (Figure 3a). This represents about 1% of the seismic data. An example of the manual annotations on inline 2587 is shown in Figure 3b, with the faults in white lineaments and the three horizons in color curves as the boundaries between four stratigraphic sequences from top to bottom. Note the missing picks of horizon no. 3 (in orange) in the deep zones, where the seismic quality is relatively low and the interpreter is not confident with providing his interpretation. It is worth mentioning that such incomplete interpretation is commonly observed in various real seismic data sets and poses a challenge in machine learning-assisted stratigraphy interpretation.

Deep CNNs

This section briefly describes how we implement the deep CNNs for fault and stratigraphy interpretation from a 3D seismic data set, with the workflows illustrated in Figures 4a and 4b, respectively. In general, both are formulated as problems of image segmentation and work by integrating two deep CNNs, with their specific implementations varying from one to the other. Specifically, for fault interpretation:

1) It is a binary classification. Correspondingly, the output is a volume of fault probability.
2) It learns from only the seismic amplitude. However, more information can be added as input if necessary.
3) The first CNN aims at identifying faults in both inline and crossline sections, which is denoted as the V-CNN for the convenience of description. It is a typical architecture of U-Net and trained using pairs of seismic and the fault labels provided on the training vertical seismic sections. In details, the V-CNN consists of a total of 30 layers and adopts the cross-entropy as loss function.
4) The second CNN, here denoted as the H-CNN, uses the merged fault

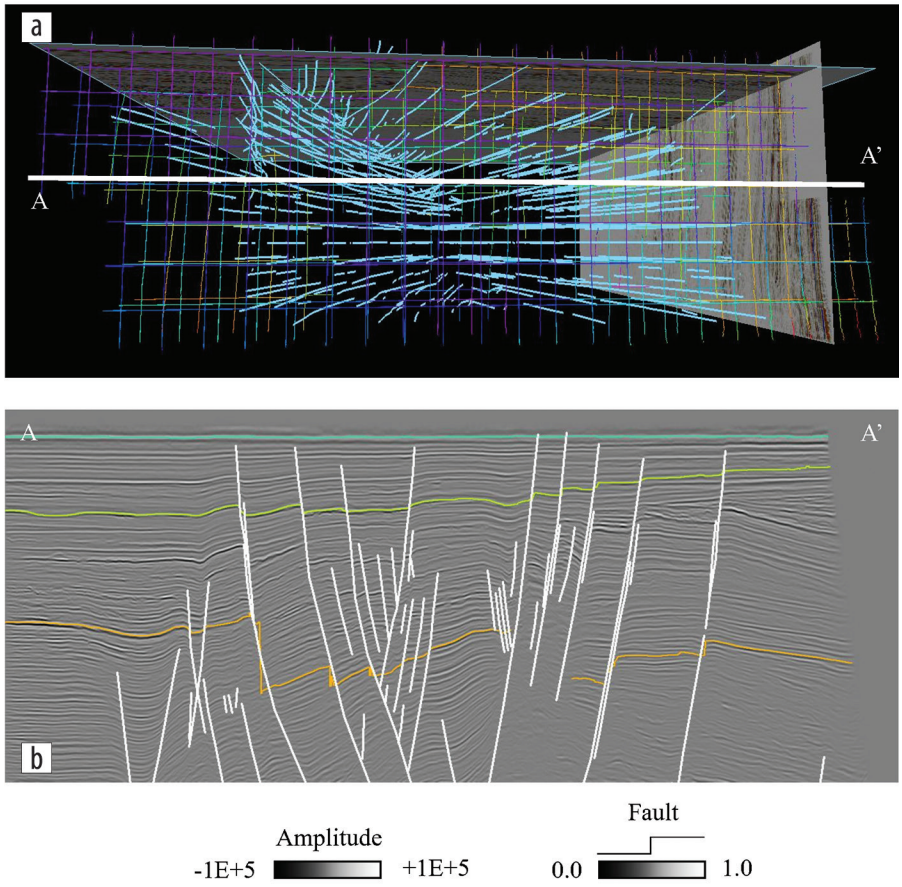

Figure 3. (a) 3D view of the seven inlines and 23 crosslines with interpreter annotations, which are used as training labels for the machine learning-assisted fault and stratigraphy interpretation. (b) An example of the fault and horizon annotations on inline section 2587.

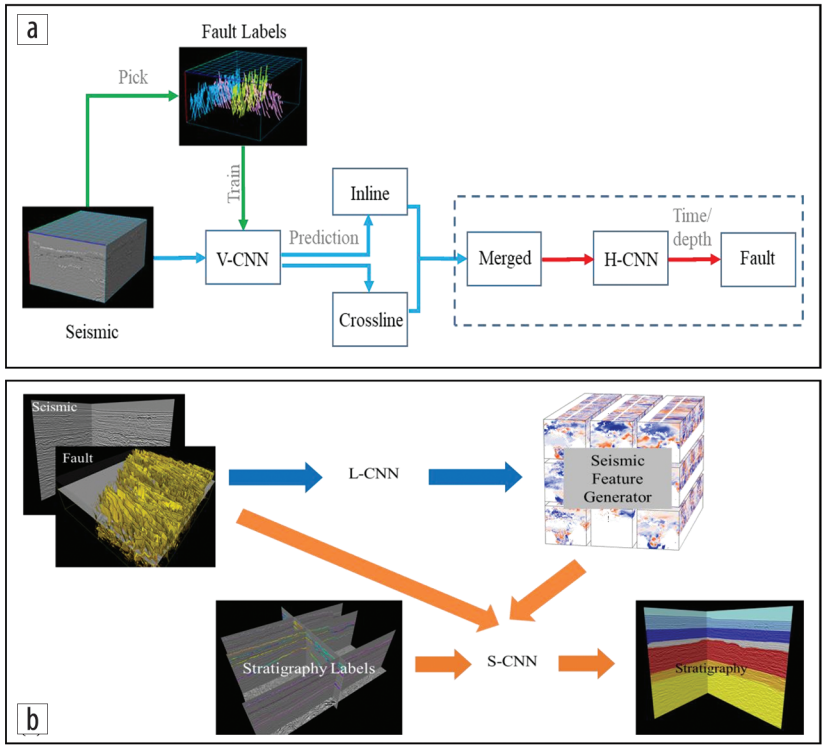

Figure 4. The workflows of deep CNN-assisted (a) fault and (b) stratigraphy interpretation, each of which consist of two deep CNNs.

prediction from the V-CNN as input and works along the horizontal direction to regroup the fault samples, which is tested capable of reducing the artifacts (i.e., isolated fault samples) and improving the lateral continuity of fault prediction. The H-CNN is also a typical architecture of U-Net but is trained using pairs of the merged V-CNN prediction and manual fault interpretation at horizontal slices. Due to no dependency on seismic amplitude, the horizontal fault grouping can be treated applicable across seismic data sets, and we have trained the H-CNN using multiple data sets. Additional training is feasible but is not performed in this case study. In details, the H-CNN consists of a total of 30 layers and adopts the cross-entropy as loss function.

More technical details about the CNN implementation for seismic fault interpretation can be found in Li and Abubakar (2019).

For stratigraphy interpretation:

1) It is a multiclass classification, with each class representing a stratigraphic sequence specified by seismic interpreters. The outputs are volumes of the probabilities of these sequences.
2) It learns from both the seismic amplitude and the fault probability generated from the previously mentioned fault workflow. In such a case, the fault information serves as an additional input for the machine to learn. Testing on multiple seismic data sets indicates its potential of optimizing the stratigraphy interpretation near the faulting zones (Di et al., 2019).
3) The first CNN aims at identifying the major seismic features in the target seismic data set by itself through self-learning, which is denoted as the L-CNN. Therefore, it requires no explicit label from interpreters and can be trained in the background while the interpreter works on generating the stratigraphy labels. As illustrated in Di et al. (2020), the impacts of such self-learning include faster convergence and better generalization for laterally consistent stratigraphy interpretation, particularly when the amount of training labels is small. In this study, the L-CNN is a typical architecture of a convolutional auto-encoder and trained using the seismic and the fault probability randomly selected on vertical sections. In details, the L-CNN consists of a total of 25 layers and adopts the mean-square-error as loss function.
4) The second CNN aims at identifying the target stratigraphic sequences in both inline and crossline sections by the provided stratigraphy labels, which is denoted as the S-CNN. However, part of it is inherited from the L-CNN. The S-CNN is also a typical architecture of U-Net and is trained using pairs of seismic as well as fault probability and the stratigraphy labels provided on the training vertical seismic sections. In details, the S-CNN consists of a total of 65 layers, with the first eight layers inherited from the pretrained L-CNN, and adopts the cross-entropy as loss function.

More technical details about the CNN implementation for seismic stratigraphy interpretation can be found in Di et al. (2020).

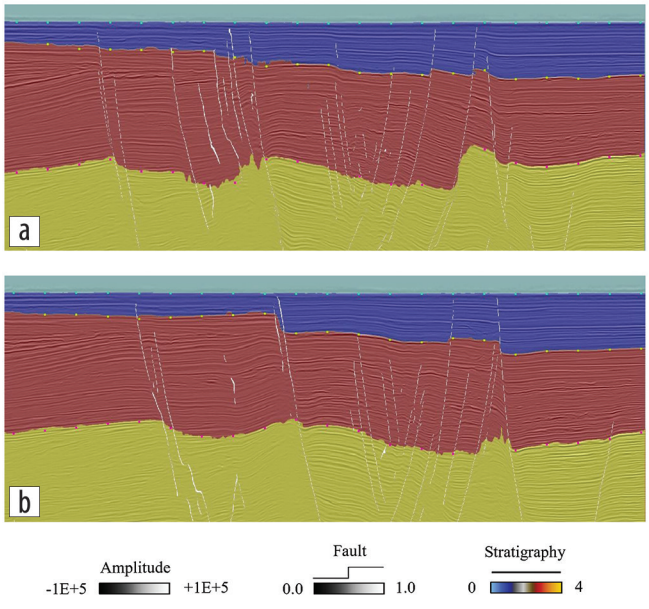

Figure 5. Fault and stratigraphy interpretation on inline 2437 and 2537, both of which are 50 inlines away, which is the maximum distance, from the nearest training sections. The color dots represent the annotation along the crossline directions as reference to verify the accuracy of the CNN interpretation.

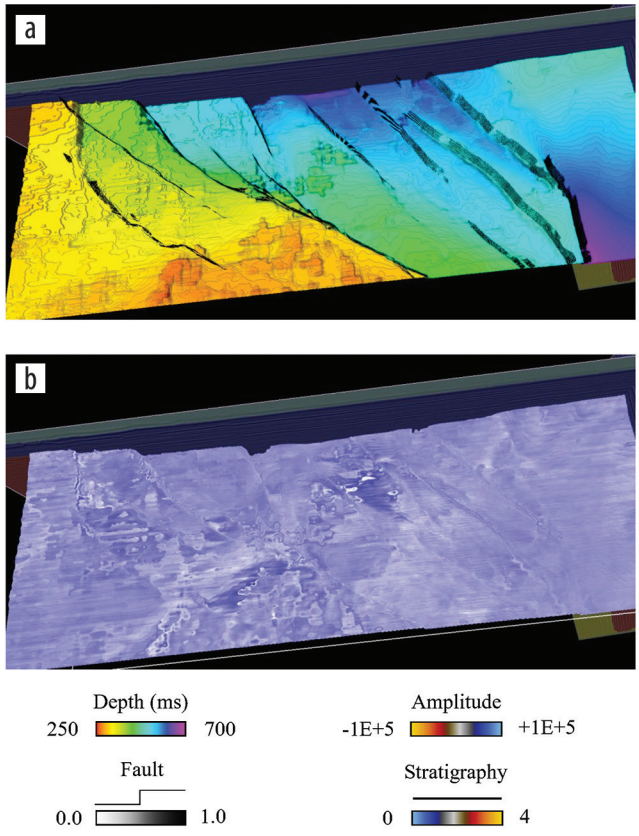

Figure 6. (a) The fault planes (in black) and the second horizon surface (in rainbow) generated from the deep CNN-assisted fault and stratigraphy interpretation, which clearly illustrates the graben structure documented in the Taranaki Basin. (b) The seismic amplitude extracted along the second horizon surface, in which the consistent seismic signature indicates good accuracy of the machine in identifying the stratigraphic boundaries.

DOI:10.1190/tle39100727.1

Result analysis

To demonstrate the results of our deep CNN-assisted fault and stratigraphy interpretation on the Opunake-3D seismic data set, we first show two inline sections (2437 and 2537) in Figure 5, with the fault in white lineaments and the four stratigraphic sequences in color zones over the original seismic amplitude. Both sections are 50 inlines, which is the maximum distance, away from the nearest training inlines. Figure 5 also displays a regular grid of dots representing the interpreter's picks of the three horizons in the crossline direction, which can serve as control points for verifying the accuracy of the stratigraphy interpretation.

Next, for evaluating the lateral consistency of the fault and stratigraphy results, we generate the boundaries between the four stratigraphic sequences from the deep CNN-assisted stratigraphy interpretation and overlay the faults from the deep CNN-assisted fault interpretation. The 3D view of the second and third boundaries is shown in Figures 6 and 7, respectively. In Figures 6a and 7a, the horizon surfaces are continuous throughout the survey, which resolves the concern of overfitting, and the fault surfaces are clearly revealed. Both interpretations are consistent with the graben structure as documented in this area. In Figures 6b and 7b, seismic amplitude is extracted along the generated horizon surfaces, and the consistent seismic signature indicates good accuracy of the machine in identifying the stratigraphic boundaries within the survey.

Conclusions

Two workflows powered by deep CNNs are implemented for automatic fault and stratigraphy interpretation in the Taranaki Basin, New Zealand. Starting from only a small amount (1%) of interpreter annotations as training labels, both workflows successfully learn the targets and generalize the learning to the entire seismic survey. The results are of high accuracy, exhibit strong lateral consistency, and are a good match with the original seismic images, which verifies the efficiency of using the deep CNN in automating the process of seismic fault and stratigraphy interpretation. Such results can be used in further analyzing the deformation and deposition history, building the 3D geologic model, and simulating the potential petroleum systems in the Taranaki Basin. TLE

Acknowledgments

Thanks go to the assistant editor Margarita Corzo, the anonymous associate editor, and three reviewers for coordinating the review process and providing insightful suggestions and comments on improving the paper quality. We would like to thank the New Zealand Crown Minerals for providing the Opunake-3D seismic data set. The deep CNNs are implemented using the open-source TensorFlow library developed by Google Brain Team.

Data and materials availability

Data associated with this research are available and can be obtained by contacting the corresponding author.

Corresponding author: hdi@slb.com

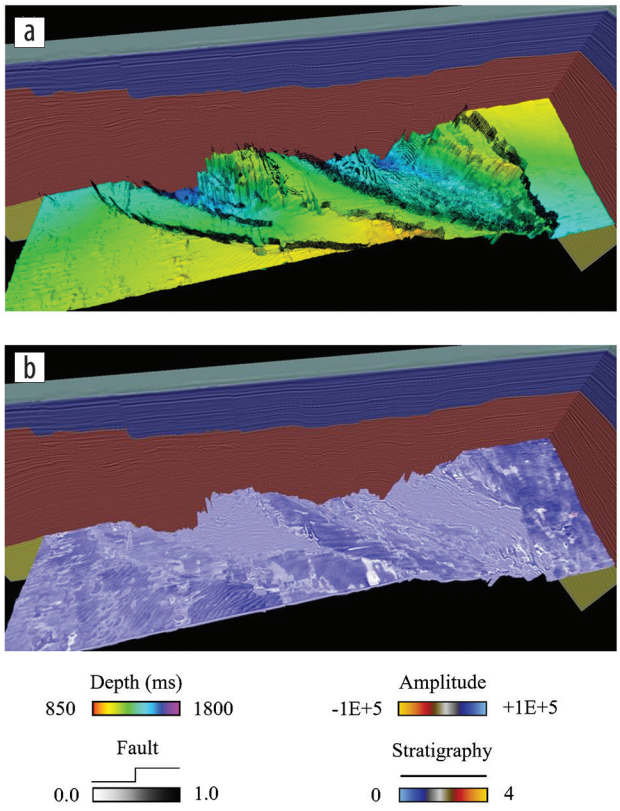

Figure 7. (a) The fault planes (in black) and the third horizon surface (in rainbow) generated from the deep CNN-assisted fault and stratigraphy interpretation, which clearly illustrates the graben structure documented in the Taranaki Basin. (b) The seismic amplitude extracted along the third horizon surface, in which the consistent seismic signature indicates the good accuracy of the machine in identifying the stratigraphic boundaries.

References

Alaudah, Y., M. Alfarraj, and G. AlRegib, 2018, Structure label prediction using similarity-based retrieval and weakly-supervised label mapping: Geophysics, **84**, no. 1, V67–V79, https://doi.org/10.1190/geo2018-0028.1.

Alaudah, Y., M. Soliman, and G. AlRegib, 2019, Facies classification with weak and strong supervision: A comparative study: 89th Annual International Meeting, SEG, Expanded Abstracts, 1868–1872, https://doi.org/10.1190/segam2019-3216766.1.

Al-Dossary, S., and K. J. Marfurt, 2006, 3D volumetric multispectral estimates of reflector curvature and rotation: Geophysics, **71**, no. 5, P41–P51, https://doi.org/10.1190/1.2242449.

AlRegib, G., M. Deriche, Z. Long, H. Di, Z. Wang, Y. Alaudah, M. A. Shafiq, and M. Alfarraj, 2018, Subsurface structure analysis using computational interpretation and learning: A visual signal processing perspective: IEEE Signal Processing Magazine, **35**, no. 2, 82–98, https://doi.org/ 10.1109/MSP.2017.2785979.

Badrinarayanan, V., A. Kendall, and R. Cipolla, 2017, SegNet: A deep convolutional encoder-decoder architecture for image segmentation: IEEE Transactions on Pattern Analysis and Machine Intelligence, **39**, no. 12, 2481–2495, https://doi.org/10.1109/TPAMI.2016.2644615.

Bahorich, M., and S. Farmer, 1995, 3-D seismic coherency for faults and stratigraphic features: The Leading Edge, **14**, no. 10, 1053–1058, https://doi.org/10.1190/1.1437077.

Di, H., and D. Gao, 2014, Gray-level transformation and Canny edge detection for 3D seismic discontinuity enhancement: Computers & Geosciences, **72**, 192–200, https://doi.org/10.1016/j.cageo.2014.07.011.

Di, H., and D. Gao, 2017, 3D seismic flexure analysis for subsurface fault detection and fracture characterization: Pure and Applied Geophysics, **174**, 747–761, https://doi.org/10.1007/s00024-016-1406-9.

Di, H., Z. Wang, and G. AlRegib, 2018, Seismic fault detection from post-stack amplitude by convolutional neural networks: 80th Conference and Exhibition, EAGE, Extended Abstracts, https://doi.org/10.3997/2214-4609.201800733.

Di, H., C. Li, S. Smith, and A. Abubakar, 2019, Machine learning-assisted seismic interpretation with geologic constraints: 89th Annual International Meeting, SEG, Expanded Abstracts, 5360–5364, https://doi.org/10.1190/segam2019-w4-01.1.

Di, H., Z. Li, H. Maniar, and A. Abubakar, 2020, Seismic stratigraphy interpretation by deep convolutional neural networks: A semisupervised workflow: Geophysics, **85**, no. 4, WA77–WA86, https://doi.org/10.1190/geo2019-0433.1.

Faraklioti, M., and M. Petrou, 2004, Horizon picking in 3D seismic data volumes: Machine Vision and Applications, **15**, 216–219, https://doi.org/10.1007/s00138-004-0151-8.

Gao, D., and H. Di, 2015, Extreme curvature and extreme flexure analysis for fracture characterization from 3D seismic data: New analytical workflows and geologic implications: Geophysics, **80**, no. 2, IM11–IM20, https://doi.org/10.1190/geo2014-0185.1.

Giba, M., A. Nicol, and J. J. Walsh, 2010, Evolution of faulting and volcanism in a back-arc basin and its implications for subduction processes: Tectonics, **29**, no. 4, TC4020, https://doi.org/10.1029/2009TC002634.

Gramstad, O., and J. Ø. H. Bakke, 2012, Seismic surface extraction using iterative seismic DNA detection: 82nd Annual International Meeting, SEG, Expanded Abstracts, https://doi.org/10.1190/segam2012-0600.1.

Guitton, A., 2018, 3D convolutional neural networks for fault interpretation: 80th Conference and Exhibition, EAGE, Extended Abstracts, https://doi.org/10.3997/2214-4609.201800732.

Hale, D., 2013, Methods to compute fault images, extract fault surfaces, and estimate fault throws from 3D seismic images: Geophysics, **78**, no. 2, O33–O43, https://doi.org/10.1190/geo2012-0331.1.

Hansen, R. J., and P. J. J. Kamp, 2004, Late Miocene to Early Pliocene stratigraphic record in northern Taranaki Basin: Condensed sedimentation ahead of Northern Graben extension and progradation of the modern continental margin: New Zealand Journal of Geology and Geophysics, **47**, no. 4, 645–662, https://doi.org/10.1080/00288306.2004.9515081.

Harrigan, E., J. R. Kroh, W. A., Sandham, and T. S. Durrani, 1992, Seismic horizon picking using an artificial neural network: IEEE International Conference on Acoustics, Speech, and Signal Processing, 105–108, https://doi.org/10.1109/ICASSP.1992.226265.

Herron, D. A., 2011, First steps in seismic interpretation: SEG, Geophysical Monograph Series no. 16, https://doi.org/10.1190/1.9781560802938.

Herron, D. A., 2015, Pitfalls in horizon autopicking: Interpretation, **3**, no. 1, SB1–SB4, https://doi.org/10.1190/INT-2014-0062.1.

Höcker, C., and G. Fehmers, 2002, Fast structural interpretation with structure-oriented filtering: The Leading Edge, **21**, no. 3, 238–243, https://doi.org/10.1190/1.1463775.

Holt, W. E., and T. A. Stern, 1991, Sediment loading on the Western Platform of the New Zealand continent: Implications for the strength of a continental margin: Earth and Planetary Science Letters, **107**, no. 3–4, 523–538, https://doi.org/10.1016/0012-821X(91)90098-3.

Holt, W. E., and T. A. Stern, 1994, Subduction, platform subsidence, and foreland thrust loading: The Late Tertiary development of Taranaki Basin, New Zealand: Tectonics, **13**, no. 5, 1068–1092, https://doi.org/10.1029/94TC00454.

Huang, K.-Y., 1997, Hopfield neural network for seismic horizon picking: 67th Annual International Meeting, SEG, Expanded Abstracts, 562–565, https://doi.org/10.1190/1.1885963.

Huang, L., X. Dong, and T. E. Clee, 2017, A scalable deep learning platform for identifying geologic features from seismic attributes: The Leading Edge, **36**, no. 3, 249–256, https://doi.org/10.1190/tle36030249.1.

Kamp, P. J. J., A. J. Vonk, K. J. Bland, R. J. Hansen, A. J. W. Hendy, A. P. McIntyre, M. Ngatai, S. J. Cartwright, S. Hayton, and C. S. Nelson, 2004, Neogene stratigraphic architecture and tectonic evolution of Wanganui, King Country, and eastern Taranaki Basins, New Zealand: New Zealand Journal of Geology and Geophysics, **47**, no. 4, 625–644, https://doi.org/10.1080/00288306.2004.9515080.

King, P. R., and G. P. Thrasher, 1996, Cretaceous-Cenozoic geology and petroleum systems of the Taranaki Basin, New Zealand: Institute of Geological and Nuclear Sciences, New Zealand Monograph 13, Ministry of Economic Development Petroleum Report 3224.

Leggett, M., W. A. Sandham, and T. S. Durrani, 1996, 3-D Seismic horizon tracking using an artificial neural network: First Break, **14**, no. 11, 413–418.

Li, C., and A. Abubakar, 2019, Interpreting seismic faults with machine learning techniques, U.S. Patent 62/853,681.

Li, Z., H. Di, H. Maniar, and A. Abubakar, 2019, Semi-supervised deep machine learning assisted seismic image segmentation and stratigraphic sequence interpretation: 81st Conference and Exhibition, EAGE, Extended Abstracts, https://doi.org/10.3997/2214-4609.201901389.

Long, J., E. Shelhamer, and T. Darrell, 2015, Fully convolutional networks for semantic segmentation: Proceedings of IEEE Conference on Computer Vision and Pattern Recognition, https://doi.org/10.1109/CVPR.2015.7298965.

Marfurt, K. J., R. L. Kirlin, S. L. Farmer, and M. S. Bahorich, 1998, 3-D seismic attributes using a semblance-based coherency algorithm: Geophysics, **63**, no. 4, 1150–1165, https://doi.org/10.1190/1.1444415.

Mattos, N. H., T. M. Alves, and A. Scully, 2019, Structural and depositional controls on Plio- Pleistocene submarine channel geometry (Taranaki Basin, New Zealand): Basin Research, **31**, no. 1, 136–154, https://doi.org/10.1111/bre.12312.

Neall, V. E, R. B. Stewart, and I. E. M. Smith, 1986, History and petrology of the Taranaki volcanoes, *in* I. E. M. Smith, ed., Late Cenozoic volcanism in New Zealand: Royal Society of New Zealand Bulletin 23, 251–264.

Nelson, C. S., P. J. J. Kamp, and H. R. Young, 1994, Sedimentology and petrography of mass-emplaced limestone (Orahiri Limestone) on a Late Oligocene shelf, western North Island, and tectonic implications for eastern margin development of Taranaki Basin: New Zealand Journal of Geology and Geophysics, **37**, no. 3, 269–285, https://doi.org/10.1080/00288306.1994.9514621.

Nicol, A., J. Walsh, K. Berryman, and S. Nodder, 2005, Growth of a normal fault by the accumulation of slip over millions of years: Journal of Structural Geology, **27**, no. 2, 327–342, https://doi.org/10.1016/j.jsg.2004.09.002.

Noh, H., S. Hong, and B. Han, 2015, Learning deconvolution network for semantic segmentation: Proceedings of IEEE International Conference on Computer Vision, https://doi.org/10.1109/ICCV.2015.178.

O'Neill, S. R., S. J. Jones, P. J. J. Kamp, R. E. Swarbrick, and J. G. Gluyas, 2018, Pore pressure and reservoir quality evolution in the deep Taranaki Basin, New Zealand: Marine and Petroleum Geology, **98**, 815–835, https://doi.org/10.1016/j.marpetgeo.2018.08.038.

Patel, D., S. Bruckner, I. Viola, and E. M. Gröller, 2010, Seismic volume visualization for horizon extraction: IEEE Pacific Visualization Symposium, https://doi.org/10.1109/PACIFICVIS.2010.5429605.

Roberts, A., 2001, Curvature attributes and their application to 3D interpreted horizons: First Break, **19**, no. 2, 85–100, https://doi.org/10.1046/j.0263-5046.2001.00142.x.

Ronneberger, O., P. Fischer, and T. Brox, 2015, U-Net: Convolutional networks for biomedical image segmentation: International Conference on Medical Image Computing and Computer-assisted Intervention, 234–241, https://doi.org/10.1007/978-3-319-24574-4_28.

Shi, Y., X. Wu, and S. Fomel, 2018, Automatic salt-body classification using a deep-convolutional neural network: 88th Annual International Meeting, SEG, Expanded Abstracts, 1971–1975, https://doi.org/10.1190/segam2018-2997304.1.

Stagpoole, V., and R. Funnell, 2001, Arc magmatism and hydrocarbon generation in the Northern Taranaki Basin, New Zealand: Petroleum Geoscience, **7**, no. 3, 255–267, https://doi.org/10.1144/petgeo.7.3.255.

Stagpoole, V., and A. Nicol, 2008, Regional structure and kinematic history of a large subduction back thrust: Taranaki Fault: Journal of Geophysical Research: Solid Earth, **113**, no. B1, https://doi.org/10.1029/2007JB005170.

Tingdahl, K. M., and M. de Rooij, 2005, Semi-automatic detection of faults in 3D seismic data: Geophysical Prospecting, **53**, no. 4, 533–542, https://doi.org/10.1111/j.1365-2478.2005.00489.x.

van Bemmel, P. P., and R. E. F. Pepper, 2000, Seismic signal processing method and apparatus for generating a cube of variance values: U.S. Patent 6,151,555.

Waldeland, A. U., A. C. Jensen, L. J. Gelius, and A. H. S. Solberg, 2018, Convolutional neural networks for automated seismic interpretation: The Leading Edge, **37**, no. 7, 529–537, https://doi.org/10.1190/tle37070529.1.

Wang, Z., H. Di, M. A. Shafiq, Y. Alaudah, and G. AlRegib, 2018, Successful leveraging of image processing and machine learning in seismic structural interpretation: A review: The Leading Edge, **37**, no. 6, 451–461, https://doi.org/10.1190/tle37060451.1.

Wu, H., B. Zhang, T. Lin, D. Cao, and Y. Lou, 2019, Semiautomated seismic horizon interpretation using the encoder-decoder convolutional neural network: Geophysics, **84**, no. 6, B403–B417, https://doi.org/10.1190/geo2018-0672.1.

Wu, X., L. Liang, Y. Shi, and S. Fomel, 2019, FaultSeg3D: Using synthetic datasets to train an end-to-end convolutional neural network for 3D seismic fault segmentation: Geophysics, **84**, no. 3, IM35–IM45.

Wu, X., and D. Hale, 2015, Horizon volumes with interpreted constraints: Geophysics, **80**, no. 2, IM21–IM33, https://doi.org/10.1190/geo2014-0212.1.

Xiong, W., X. Ji, Y. Ma, Y. Wang, N. M. AlBinHassan, M. N. Ali, and Y. Luo, 2018, Seismic fault detection with convolutional neural network: Geophysics, **83**, no. 5, O97–O103, https://doi.org/10.1190/geo2017-0666.1.

Yu, Y., C. Kelley, and I. Mardanova, 2008, Seismic horizon autopicking using orientation vector field: U.S. Patent 8,265,876.

Yu, Y., C. Kelley, and I. Mardanova, 2011, Automatic horizon picking in 3D seismic data using optical filters and minimum spanning tree (patent pending): 81st Annual International Meeting, SEG, Expanded Abstracts, 965–969, https://doi.org/10.1190/1.3628233.

Zeiler, M. D., G. W. Taylor, and R. Fergus, 2011, Adaptive deconvolutional networks for mid and high level feature learning: Proceedings of IEEE International Conference on Computer Vision, https://doi.org/10.1109/ICCV.2011.6126474.